

Reactions of a {Mo₁₆}-type polyoxometalate cluster with electrophiles: a synthetic, theoretical and magnetic investigation

De-Liang Long,^a Paul Kögerler,^b Louis J. Farrugia^a and Leroy Cronin^{*a}

^a Department of Chemistry, The University of Glasgow, Glasgow, UK G12 8QQ.

E-mail: L.Cronin@chem.gla.ac.uk

^b Ames Laboratory and Department of Physics & Astronomy, Iowa State University, Ames, IA 50011, USA

Received 5th January 2005, Accepted 2nd February 2005

First published as an Advance Article on the web 17th March 2005

A medium-nuclearity mixed-valence polyoxomolybdate [H₂Mo₁₆O₅₂]¹⁰⁻ = {Mo₁₆} (**1a**) was synthesized using an approach that employed protonated hexamethylenetetramine (HMTAH⁺) as counter ion and yielded (HMTAH)₁₀ **1a**·34 H₂O (**1**). The {Mo₁₆} cluster anion exhibits significant nucleophilicity and traps electrophiles such as divalent transition metal ions, resulting in a family of isostructural compounds based on {Mo₁₆M₂}-type anions [M(H₂O)₈H₂Mo₁₆O₅₂]⁶⁻ (M = Fe^{II} (**2**), Mn^{II} (**3**), Co^{II} (**4**)). The highly reactive nature of the {Mo₁₆} system is also revealed by rearrangement and decomposition reactions of **1** to either slowly form a sodium-bridged heptamolybdate-based chain compound (**5**) when left in the reaction solution or, in the presence of very high concentrations of electrophiles, to heptamolybdate-based cluster compounds [M₂(H₂O)₉Mo₇O₂₄]²⁻ of the {M₂Mo₇}-type (M = Fe^{II} (**6**), Mn^{II} (**7**)). Compounds **1–7** were characterised by single crystal X-ray diffraction, elemental analysis, IR spectroscopy, magnetic susceptibility measurements, and density functional theory calculations.

Introduction

The self-assembly of polyoxometalate-based coordination compounds provides a convenient approach to molecular metal oxide architectures based on molybdenum, tungsten, or vanadium.¹ Indeed, their versatile nature originates from the ability to link oxo-anions into a range of clusters including ultra-large clusters containing several hundred metal ions in a single molecule.² Given the range of accessible structures, and their attractive and almost unmatched range of electronic and molecular properties, polyoxometalates (POMs) have been the subject of an immense number of studies in many fields including catalysis,^{3,4} magnetism,^{5,6} medicinal chemistry,^{7,8} and materials science.^{9–11} Thus research towards understanding and manipulation of the self assembly processes that underpin the formation of POM clusters has to be an attractive route to enable the design of designer clusters and multi-functional materials, which take advantage of the unique physical properties associated with this extraordinary class of molecules.¹²

The routes to synthesize POM clusters (large or small) often employ 'one-pot' reactions.^{1–3} As such, the manipulation of some of the many reaction parameters often represents a straight-forward, but rather serendipitous, route to new, self-assembled POM architectures.¹ One potential avenue of investigation that may allow the design of larger architectures based on clusters uses POM building blocks as synthons.¹³ This is because the ability to assemble large cluster systems from smaller known building blocks could be a direct way to systematically control the overall cluster architecture and properties while retaining the geometries of the building blocks. Thus, such building blocks of well-defined shape and connectivity might form the basis for work towards the growth of nanoscopic clusters of predetermined structure and function. However, the major problem with this approach lies in establishing routes to produce reactive building blocks present in solution in significant concentrations that can be reliably utilized in the formation of larger architectures, without re-organizing to other unknown fragments. Access to such building blocks has been the major limitation in stepwise growth of Mo-based POM clusters compared to the more kinetically inert W-based clusters.¹⁴ Such

limitations may be circumvented by adopting an approach that kinetically stabilizes the building block in solution, thereby effectively preventing its reorganization to other structure types.

One possible route to this goal is to use bulky organic cations to isolate new structure types by virtue of the cations used to 'encapsulate' the new building blocks, thereby limiting their reorganization to simpler structural types. By trapping clusters during the self-assembly process it may be possible to restrain the cluster from reorganizing into other well-known structure types. Also, in many cases, synthetic strategies toward Mo-based cluster systems are guided by the fact that structures of polyoxomolybdate clusters are frequently derived from highly stable, low-nuclearity structural archetypes such as the *O_h*-symmetric Lindqvist¹⁵ anion [Mo₆O₁₉]²⁻ and the various isomers of the Keggin structure,¹⁶ [Mo₁₂O₃₆(XO₄)]ⁿ⁻, or the Dawson structure,¹⁷ [Mo₁₈O₄₆(XO₄)₂]ⁿ⁻ (X = S, P, As, Si *etc.*). Templated or non-templated by main-group hetero anions, these anions all generally adopt a spherical shape, and so are the very few known polyoxomolybdate anions of {Mo₁₆} nuclearity. For example, [NaMo₁₆(OH)₁₂O₄₀]⁷⁻ and [H₂Mo₁₆(OH)₁₂O₄₀]^{6–18,19} exhibit cluster structures based on the fully reduced ϵ -Keggin {Mo^V₁₂} motif with four capping [Mo^{VI}O₃] units.

Previously, by using protonated hexamethylenetetramine (HMTAH⁺) as counter ions, we were able to stabilize and isolate a highly charged polyoxomolybdate anion, [H₂Mo^V₄Mo^{VI}₁₆O₅₂]¹⁰⁻ **1a**, which represents a new structural type.²⁰ The anion **1a** displays an unusual flat shape and can itself be formally decomposed into a highly condensed {Mo₁₂} building block which incorporates two pairs of Mo^V centres and to which two edge-sharing {Mo₂} groups are attached *via* corners. As we previously reported, **1a** is stable in the solid state as the salt (C₆H₁₃N₄)₁₀[H₂Mo₁₆O₅₂]¹⁰⁻·34H₂O (**1**) since the highly negative cluster anion is virtually completely wrapped by the organic HMTAH⁺ cations. In an extension to this approach we also recently isolated a family of sulfite-based Dawson-type mixed-valence polyoxomolybdates [Mo₁₈O₅₄(SO₃)₂]ⁿ⁻, using the same type of synthetic approach. Furthermore these [Mo₁₈O₅₄(SO₃)₂]ⁿ⁻ clusters possess unusual electronic properties and display S···S interactions between the lone pairs of the two sulfite anions inside the cluster.²¹ Thus, the use of bulky

organic cations in the formation of Mo-based POMs appears to restrict aggregation to the more highly symmetrical cluster types, allowing a fundamentally more diverse set of clusters and cluster-based building blocks to be isolated, that display unprecedented structural^{20,22} or physical²¹ features. Herein, we report a full investigation into the $[\text{H}_2\text{Mo}^{\text{V}}_4\text{Mo}^{\text{VI}}_{16}\text{O}_{52}]^{10-}$ system and its reactivity towards electrophiles, as well as investigations into the magnetic and electronic properties. Our results demonstrate that the $[\text{H}_2\text{Mo}^{\text{V}}_4\text{Mo}^{\text{VI}}_{16}\text{O}_{52}]^{10-}$ structure is indeed kinetically stabilized by the presence of a surrounding sheath of the bulky HMTAH⁺ cations, and also can be stabilized further after it coordinates two divalent metal cations to two specific binding sites.

Experimental

General procedures

All reagents and chemicals were purchased from commercial sources and used without further purification. Infrared spectra were recorded as KBr discs using a Perkin-Elmer paragon 1000 PC or Nicolet Magna 550 series II FTIR spectrometer. Magnetic susceptibility measurements were performed using a Quantum Designs MPMS-5 SQUID magnetometer. Variable temperature (2–290 K) susceptibilities were recorded at 0.5 Tesla. In addition, field-dependent (0.1–5.0 Tesla) measurements of all compounds at 10 K showed linear M vs. H behaviour and excluded the presence of a significant amount of magnetic impurities. Susceptibilities were corrected for diamagnetic and temperature-independent paramagnetism (TIP) contributions that were derived from a combination of Pascal's constants and the experimentally determined diamagnetic susceptibility of compounds **1** with $\chi_{\text{dia/TIP}}(\mathbf{1}) = -1.03 \times 10^{-3}$ emu mol⁻¹ (for compounds **2–4**) and **5** with $\chi_{\text{dia/TIP}}(\mathbf{5}) = -3.48 \times 10^{-4}$ emu mol⁻¹ (for compounds **6** and **7**). This approach is necessary as the simple addition of Pascal's constants does not incorporate TIP effects and thus largely overestimates $\chi_{\text{dia/TIP}}$ values for most polyoxomolybdate compounds.

Density functional theory calculations (including Löwdin and Mulliken population analysis) using the TURBOMOLE 5.6 program suite required TZVPP (cc-pVTZ polarization functions) basis sets and hybrid B3-LYP exchange–correlation functionals to converge. All structures were based on crystallographic coordinates that were allowed to equilibrate without symmetry restrictions; the coordinates for the Fe^{II}-based anion **2a** were used for the $\{\text{Zn}_2\text{Mo}_{16}\}$ derivative. The maximum shift for each atomic position generated by the free geometric equilibration amounted to 0.10 Å, which was mainly observed for terminal oxygen positions.

Synthetic procedures

Synthesis of $(\text{C}_6\text{H}_{13}\text{N}_4)_{10}[\text{H}_2\text{Mo}_{16}\text{O}_{52}]\cdot 34\text{H}_2\text{O}$ **1.** Hexamethylenetetraamine (2.2 g, 15.7 mmol) was dissolved in water (20 ml) and acidified by addition of hydrochloric acid (37%, 1.2 ml). Subsequently, $\text{Na}_2\text{MoO}_4 \cdot 2\text{H}_2\text{O}$ (0.96 g, 4.0 mmol) and $\text{Na}_2\text{S}_2\text{O}_4$ (0.07 g, 0.44 mmol) were added to the reaction solution simultaneously with stirring. The solution colour changes to green initially, then to yellowish green, and finally to brown. The resulting solution was filtered and sealed in a vial and was left to stand for two days after which time brown crystals appeared. Yield: 0.20 g (18%, all yields calculated based on molybdenum). IR (KBr disk): 3443, 1631, 1461, 1400, 1378, 1308, 1289, 1253, 1203, 1018, 1009, 978, 926, 817, 794, 658 cm⁻¹; elemental analysis calcd. for $\text{C}_{60}\text{H}_{200}\text{Mo}_{16}\text{N}_{40}\text{O}_{86}$: C 16.40, H 4.59, N 12.75; found: C 16.28, H 4.13, N 12.77%. Replacing hydrochloric acid with sulfuric acid yields the same product in this synthesis. Using pure acetic acid to acidify hexamethylenetetraamine solution quickly produces an unknown precipitate. Acetic acid can still be successfully integrated into this reaction system in a combination process that initially uses 0.8 ml hydrochloric acid (37%). After

the addition of $\text{Na}_2\text{MoO}_4 \cdot 2\text{H}_2\text{O}$ and $\text{Na}_2\text{S}_2\text{O}_4$ the reaction solution is acidified further by 0.5 ml of acetic acid (100%); note that this does not result in the incorporation of acetate ions in the product as only pure **1** is formed.

Synthesis of $(\text{C}_6\text{H}_{13}\text{N}_4)_6[\text{Fe}_2(\text{H}_2\text{O})_8\text{H}_2\text{Mo}_{16}\text{O}_{52}]\cdot 8\text{H}_2\text{O}$ **2.** The brown reaction solution obtained, as for the synthesis of **1**, was kept undisturbed for 6 h. After this period it was added into a solution of $\text{FeSO}_4 \cdot 7\text{H}_2\text{O}$ (0.18 g, 0.65 mmol) in H_2O (50 ml), which was acidified by using hydrochloric acid (37%, 0.20 ml). The mixture was stirred for two minutes and quickly filtered. The solution colour slightly changed from brown to reddish brown. Deep brown strip crystals were obtained overnight. Yield: 0.25 g (28%). IR (KBr disk): 3426, 1637, 1462, 1401, 1384, 1259, 1017, 980, 925, 887, 639 cm⁻¹; elemental analysis calcd. for $\text{C}_{36}\text{H}_{112}\text{Fe}_2\text{Mo}_{16}\text{N}_{24}\text{O}_{68}$: C 11.96, H 3.12, N 9.30; found: C 11.90, H 3.00, N 8.96%.

Synthesis of $(\text{C}_6\text{H}_{13}\text{N}_4)_6[\text{Mn}_2(\text{H}_2\text{O})_8\text{H}_2\text{Mo}_{16}\text{O}_{52}]\cdot 8\text{H}_2\text{O}$ **3 and $(\text{C}_6\text{H}_{13}\text{N}_4)_6[\text{Co}_2(\text{H}_2\text{O})_8\text{H}_2\text{Mo}_{16}\text{O}_{52}]\cdot 8\text{H}_2\text{O}$ **4**.** Deep brown crystals of **3** and **4** were produced in the same procedure as used for synthesis of **2** by replacing $\text{FeSO}_4 \cdot 7\text{H}_2\text{O}$ with $\text{MnSO}_4 \cdot \text{H}_2\text{O}$ (0.08 g, 0.50 mmol) or $\text{CoCl}_2 \cdot 6\text{H}_2\text{O}$ (0.18 g, 0.75 mmol), respectively. For **3**, yield: 0.21 g (23%). IR (KBr disk): 3454, 1638, 1462, 1406, 1365, 1259, 1219, 1066, 1018, 980, 962, 925, 887 cm⁻¹; elemental analysis calcd. for $\text{C}_{36}\text{H}_{112}\text{Mn}_2\text{Mo}_{16}\text{N}_{24}\text{O}_{68}$: C 11.96, H 3.12, N 9.30; found: C 11.68, H 2.90, N 8.98%. For **4**, yield: 0.24 g (27%). IR (KBr disk): 3406, 1637, 1462, 1403, 1379, 1259, 1018, 980, 925, 885, 795, 640 cm⁻¹; elemental analysis calcd. for $\text{C}_{36}\text{H}_{112}\text{Co}_2\text{Mo}_{16}\text{N}_{24}\text{O}_{68}$: C 11.94, H 3.12, N 9.28; found: C 11.65, H 3.00, N 8.84%.

Synthesis of $(\text{C}_6\text{H}_{14}\text{N}_4)_{1.5}(\text{C}_7\text{H}_{17}\text{N}_5)_{0.5}[\text{Na}_2(\text{H}_2\text{O})_5\text{Mo}_7\text{O}_{24}]\cdot 4\text{H}_2\text{O}$ **5.** Crystals of **5** were obtained from the reaction system that yields compound **1**. After crystals of **1** were formed, the solution was left undisturbed over a period of a week during which time the crystals of **1** gradually dissolved and large pale green crystals of **5** formed. Yield: 0.65 g (73%). IR (KBr disk): 3426, 1631, 1432, 1314, 1259, 1153, 1041, 1014, 993, 892, 843, 669 cm⁻¹; elemental analysis calcd. for $\text{C}_{12.5}\text{H}_{47.5}\text{Mo}_7\text{N}_{8.5}\text{Na}_2\text{O}_{33}$: C 9.61, H 3.06, N 7.62; found: C 9.42, H 3.11, N 7.10%.

Synthesis of $(\text{C}_6\text{H}_{13}\text{N}_4)_2[\text{Fe}_2(\text{H}_2\text{O})_9\text{Mo}_7\text{O}_{24}]\cdot 2\text{H}_2\text{O}$ **6.** Crystals of **6** were produced as follows: The brown reaction solution obtained during the synthesis of **1** was kept undisturbed for 6 h. After this period it was quickly mixed with a solution of $\text{FeSO}_4 \cdot 7\text{H}_2\text{O}$ (0.90 g, 3.2 mmol) in H_2O (50 ml), which was acidified previously using hydrochloric acid (37%, 0.20 ml). The mixture was stirred for 2 minutes and quickly filtered. The colour of the solution slightly changed from brown to reddish brown. Dark brown block crystals were obtained overnight. Yield: 0.24 g (26%). IR (KBr disk): 3207, 1637, 1462, 1405, 1372, 1255, 1023, 979, 934, 892, 841, 660 cm⁻¹; elemental analysis calcd. for $\text{C}_{12}\text{H}_{48}\text{Fe}_2\text{Mo}_7\text{N}_8\text{O}_{35}$: C 8.75, H 2.94, N 6.80; found: C 9.23, H 2.85, N 6.81%.

Synthesis of $(\text{C}_6\text{H}_{13}\text{N}_4)_2[\text{Mn}_2(\text{H}_2\text{O})_9\text{Mo}_7\text{O}_{24}]\cdot 2\text{H}_2\text{O}$ **7.** Crystals of **7** were produced in a synthesis route analogous to that of **6**. The initial brown reaction solution obtained in the synthesis of **1** was kept undisturbed for 6 h. Then it was stirred into a solution of $\text{MnAc}_2 \cdot 4\text{H}_2\text{O}$ (1.25 g, 5.1 mmol) in H_2O (50 ml). The mixture was stirred for 2 minutes and quickly filtered. A grey precipitate was obtained and light green crystals were obtained a few days later. Yield: 0.35 g (38%). IR (KBr disk): 3211, 1637, 1466, 1372, 1305, 1255, 1214, 1024, 976, 934, 894, 850, 680 cm⁻¹; elemental analysis calcd. for $\text{C}_{12}\text{H}_{48}\text{Mn}_2\text{Mo}_7\text{N}_8\text{O}_{35}$: C 8.76, H 2.94, N 6.81; found: C 8.96, H 2.97, N 6.99%.

Synthesis of $(\text{C}_6\text{H}_{13}\text{N}_4)_6[\text{Zn}_2(\text{H}_2\text{O})_8\text{H}_2\text{Mo}_{16}\text{O}_{52}]\cdot 8\text{H}_2\text{O}$ **8 and $(\text{C}_6\text{H}_{13}\text{N}_4)_6[\text{Ni}_2(\text{H}_2\text{O})_8\text{H}_2\text{Mo}_{16}\text{O}_{52}]\cdot 8\text{H}_2\text{O}$ **9**.** Powder samples of **8** and **9** were produced in the same procedure as used for synthesis of **2** by replacing $\text{FeSO}_4 \cdot 7\text{H}_2\text{O}$ with ZnCl_2 (0.12 g, 0.88 mmol) or $\text{NiCl}_2 \cdot 6\text{H}_2\text{O}$ (0.18 g, 0.76 mmol), respectively.

Grey precipitates were formed immediately after zinc and nickel salt solutions were mixed into the molybdate solution. These precipitates were filtered off and dried under vacuum. For **8**, yield: 0.32 g (36%). IR (KBr disk): 3205, 1636, 1462, 1404, 1362, 1258, 1219, 1065, 1010, 980, 960, 918, 875 cm⁻¹; elemental analysis calcd. for C₃₆H₁₁₂Mo₁₆N₂₄O₆₈Zn₂: C 11.89, H 3.11, N 9.25; found: C 11.68, H 2.99, N 8.92%. For **9**, yield: 0.25 g (28%). IR (KBr disk): 3423, 1638, 1463, 1401, 1401, 1261, 1016, 980, 937, 870, 794, 651 cm⁻¹; elemental analysis calcd. for C₃₆H₁₁₂Mo₁₆N₂₄Ni₂O₆₈: C 11.94, H 3.12, N 9.28; found: C 10.49, H 2.77, N 8.20%. The X-ray powder diffraction pattern of compound **8** is identical to that simulated from the single crystal structure of **2**. This implies compound **8** has the same framework structure as that of **2** with zinc ions replacing the position of iron sites. Elemental analysis also confirmed compound **8** as a pure single phase. Although few single crystals were obtained from the mother liquor for the nickel analogue that had unit cell dimensions similar to those of compound **2** (as determined by single crystal diffraction but the crystal diffracted too weakly to enable a full data collection), X-ray powder diffraction, elemental analysis and magnetic measurements indicated that the quickly deposited powder of compound **9** contains a large fraction of an unidentified impurity.

Crystallographic structure determinations

Details of data collection procedures and structure refinements are given in Table 1. Single crystals of suitable size were attached to glass fibres using Fomblin YR-1800 oil, and mounted on a goniometer head in a general position. Some samples suffered solvent loss, this being particularly severe for compound **1**, which required that these crystals were glued to the glass fibre under solvent and transferred as rapidly as possible to the cold stream of the Oxford Instruments Cryostream. All data were collected on a Nonius KappaCCD diffractometer, equipped with graphite monochromated X-radiation ($\lambda = 0.71073$ Å), running under the Collect software. The structures were solved by SHELXS-97.²³ All non-hydrogen atoms were refined anisotropically and the hydrogen atoms were fixed with C–H = 0.96 Å, and were refined with a riding model and with U_{iso} set to 1.2 times that of the attached C atom. Refinement was with SHELXL-97 using full-matrix least-squares on F^2 and all the unique data. All samples showed the presence of disordered solvent molecules. All calculations were carried out using the WinGX package²⁴ of crystallographic programs.

CCDC reference numbers 205853 (**1**),²⁰ 205854 (**2**),²⁰ 259742 (**3**), 259743 (**4**), 259744 (**5**), 259745 (**6**) and 259746 (**7**).

See <http://www.rsc.org/suppdata/dt/b4/b419301f/> for crystallographic data in CIF or other electronic format.

Results and discussion

Synthetic strategy

Crystals of [C₆H₁₃N₄]₁₀[H₂Mo₁₆O₅₂]₁₀·34H₂O **1** were obtained from a buffered solution with a pH of around 4.0 that utilises protonated HMTA as counter ions. Normally, medium- and high-nuclearity polyoxomolybdates are formed at lower pH values such as 1 to 2. However, it was observed that the combination of HMTA and molybdate in a solution at a pH value of 4 and below produces a white precipitate that is not able to form soluble 'molybdenum blue'-type solutions.³² Therefore, the reaction was carried out at the lowest possible pH (before precipitation occurs) of around 4. Also, the reducing agent Na₂S₂O₄ was added simultaneously with the addition of sodium molybdate which allows the quick formation of soluble reduced polyoxomolybdate species. Following the formation of [H₂Mo₁₆O₅₂]¹⁰⁻, further acidification of the solution causes the {Mo₁₆} cluster to decompose and causes precipitation. This precipitate was confirmed to be the same phase as compound **5** by X-ray powder diffraction analysis. Furthermore, it was

observed that compound **5** is either produced during the formation of **1** in a competing reaction that involves Na⁺ cations or by decomposition of **1** in the presence of the mother liquor; this decomposition appears to be accelerated upon heating. The reactions that produce compounds **6** and **7** were originally designed for synthesising similar cluster compounds of **2** and **3** but with more Fe²⁺ or Mn²⁺ ions attached to the molybdate cluster [H₂Mo₁₆O₅₂]¹⁰⁻. However, **1** decomposed when the Fe²⁺ or Mn²⁺ ion concentrations are increased, yielding metal complexes of heptamolybdate. Medium Fe²⁺ concentrations result in mixtures of **2** and **6** as confirmed by X-ray powder diffraction or **3** and **7** for Mn²⁺. Bridging anions such as acetate and sulfate have occasionally been reported to involve in the formation of polymolybdates.^{26–29} To explore their effect in the present system in the presence of protonated HMTA, we have probed the use of sulfuric acid or a combination of hydrochloric and acetic acid (complete acidification by acetic acid results in the rapid precipitation of an unknown compound), but this approach yields the same product of **1** rather than products containing acetate or sulfate.

Structural analysis

The crystal structure of **1** comprises discrete centrosymmetric anions [H₂Mo^V₄Mo^{VI}₁₂O₅₂]¹⁰⁻ **1a**, HMTAH⁺ cations and crystal water molecules. The [H₂Mo₁₆O₅₂]¹⁰⁻ anions contain four formal Mo^V centres that are organized as two inversion symmetry-related {Mo₂} pairs in the cluster's centre with short Mo...Mo distances of 2.612(2) Å. Such {Mo₂} motifs are typical for mixed-valence polyoxomolybdate structures and responsible for the dark brown colour of **1**.³³ The Mo^V₄Mo^{VI}₁₂ reduction state has also been confirmed by redox titrations and the Mo^V centres can be identified unambiguously from a bond valence sum analysis. In contrast to well-known archetypal polyoxomolybdate structures such as the Lindqvist anion [Mo₆O₁₉]²⁻, the Keggin anion α -[Mo₁₂O₃₆(PO₄)₃]³⁻, or the Dawson anion α -[Mo₁₈O₅₄(PO₄)₂]⁶⁻ which all are characterized by their spherical shapes, **1a** displays a plate-like geometry with a length of ~13 Å, width ~11 Å and thickness of ~6 Å. The degree of condensation of the sixteen MoO₆ octahedra in **1a** allows us to formally decompose the cluster into a central {Mo₁₂} building block and two {Mo₂} groups that are adjoined to the sides of and sharing corners with the {Mo₁₂} group, see Fig. 1. Eight Mo positions of the {Mo₁₂} building block arrange along two lines to form two inversion-related 'backbones'. The other four molybdenum centres at the ends of the two 'backbones' unite the two 'backbones' through bridging oxo ligands. The two Mo centres of each {Mo₂} group are bridged *via* a μ_2 -oxo and a μ_2 -hydroxo function and coordinate to two terminal and two μ_2 -oxo positions of the {Mo₁₂} fragment building blocks. Although {Mo₂}-type building blocks are abundant in various other large polyoxomolybdates such as clusters based on the doughnut-shaped {Mo₅₇M₆} structural type or the giant ring clusters of the type {Mo₁₅₄} and {Mo₁₇₆} and their derivatives, these consist of either two corner-shared Mo^{VI}O₆ octahedra (found in the giant ring molecules) or comprise reduced Mo^V centres. {Mo₂} building blocks consisting of edge-sharing Mo^{VI}O₆ octahedra, on the other hand, are seen for the first time in the {Mo₁₆} structural motif. For the complete cluster, terminal Mo=O bonds with bond lengths in the range of 1.6 to 1.7 Å are found, while the bridging Mo–O bond lengths of bridging oxygen centres range from 1.7 to 2.2 Å. Further, some of the terminal oxygen centres form hydrogen bonds with solvated water molecules and the protonated HMTA cations.

Interestingly, the arrangement of the sixteen Mo positions bears similarities to the metal skeleton found for the cluster molecule {Mn₁₆}, [Mn₁₆O₁₆(OMe)₆(OAc)₁₆(MeOH)₃(H₂O)₃·6H₂O, see Fig. 2,²⁵ although both molecules differ in the coordinating modes of their ligands.

Table 1 Crystallographic data collection, intensity measurements and structure refinement parameters for 1–7 (note that structures 1 and 2 have been reported by us in an earlier publication and are included here for comparative purposes)²⁰

	1	2	3	4	5	6	7
Chemical formula	C ₆₀ H ₃₀₀ Mo ₁₆ N ₄₀ O ₈₆	C ₃₆ H ₁₁₂ Fe ₂ Mo ₁₆ N ₂₄ O ₈₈	C ₃₆ H ₁₁₂ Mn ₂ Mo ₁₆ N ₂₄ O ₈₈	C ₃₆ H ₁₁₂ Co ₂ Mo ₁₆ N ₂₄ O ₈₈	C _{12.5} H _{37.5} Mo ₇ N _{3.5} Na ₂ O ₃₃	C ₁₂ H ₄₈ Fe ₂ Mo ₇ N ₈ O ₃₅	C ₁₂ H ₄₈ Mn ₂ Mo ₇ N ₈ O ₃₅
<i>M</i> /g mol ⁻¹	4393.64	3616.24	3614.42	3622.40	1562.65	1647.86	1646.04
Symmetry	Triclinic	Monoclinic	Monoclinic	Monoclinic	Orthorhombic	Monoclinic	Monoclinic
Space group	<i>P</i> $\bar{1}$	<i>P</i> ₂ / <i>a</i>	<i>P</i> ₂ / <i>a</i>	<i>P</i> ₂ / <i>a</i>	<i>Pnma</i>	<i>C</i> 2/ <i>c</i>	<i>C</i> 2/ <i>c</i>
<i>a</i> /Å	13.8178(1)	13.8732(1)	13.9822(1)	13.8350(6)	14.5968(2)	43.3614(5)	43.6128(4)
<i>b</i> /Å	16.1705(2)	25.6770(2)	25.7326(2)	25.7420(11)	18.6325(3)	12.3987(2)	12.4342(1)
<i>c</i> /Å	17.0835(2)	15.87270(10)	15.78750(10)	15.8150(7)	15.3796(2)	16.2413(2)	16.2899(1)
<i>a</i> /°	95.1180(10)	90	90	90	90	90	90
<i>β</i> /°	112.5320(10)	108.8090(10)	108.7940(10)	108.594(2)	90	111.4250(10)	111.2008(3)
<i>γ</i> /°	96.7450(10)	90	90	90	90	90	90
<i>V</i> /Å ³	3463.68(6)	5328.66(7)	5377.46(7)	5338.4(4)	4182.87(10)	8128.33(19)	8235.95(11)
<i>Z</i>	1	2	2	2	4	8	8
<i>D</i> _x /g cm ⁻³	2.106	2.254	2.232	2.254	2.481	2.693	2.655
<i>μ</i> /mm ⁻¹	1.513	2.182	2.128	2.217	2.165	2.898	2.769
<i>F</i> (000)	2200	3528	3524	3532	3048	6416	6400
Crystal size/mm	0.25 × 0.20 × 0.09	0.47 × 0.35 × 0.03	0.49 × 0.32 × 0.04	0.45 × 0.30 × 0.02	0.20 × 0.05 × 0.05	0.40 × 0.40 × 0.30	0.40 × 0.30 × 0.20
No. data measured	76303	79325	67322	44106	50728	22456	65968
No. unique data	20204	10413	10550	9752	4710	7982	9310
No. observed data	16176	9399	9233	7163	3755	7558	9111
No. variables	910	758	738	658	320	590	595
<i>R</i> 1	0.0368	0.0371	0.0403	0.0595	0.0373	0.0447	0.0447
<i>R</i> 2 (all data)	0.0826	0.1035	0.1137	0.1593	0.1039	0.1015	0.1089
Goodness of fit, <i>S</i>	1.029	1.085	1.095	1.158	1.070	1.338	1.378
Maximum shift/error	0.001	0.002	0.001	0.001	0.001	0.002	0.002

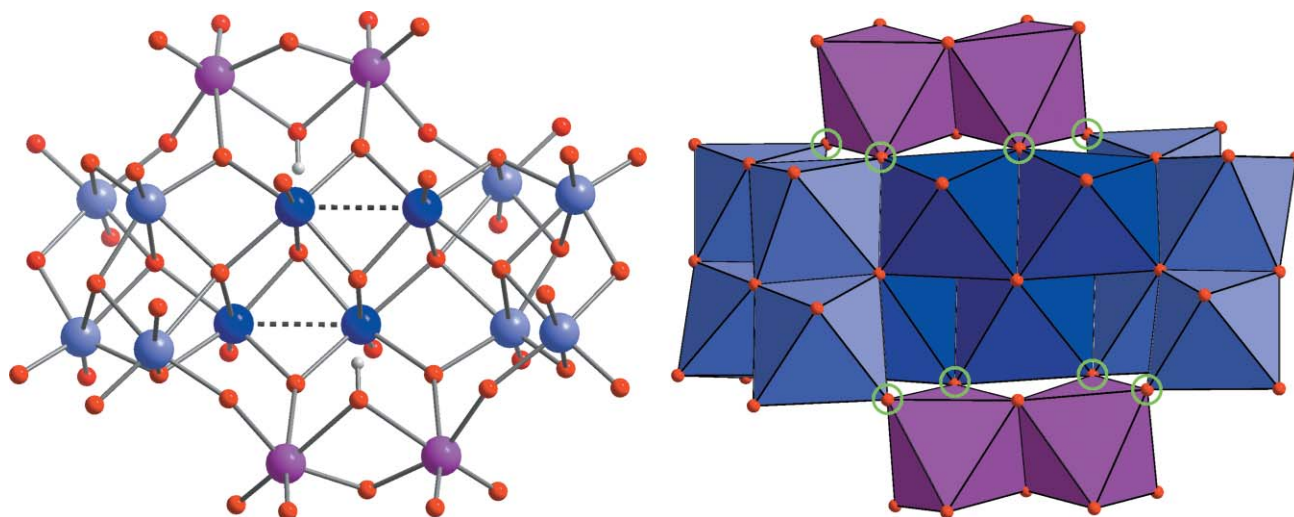


Fig. 1 Left: Ball-and-stick representation of the molecular structure of $[\text{H}_2\text{Mo}_{16}\text{O}_{52}]^{10-}$ **1a** (Mo^{VI} centres of the central $\{\text{Mo}_{12}\}$ building block: bright blue; Mo^{V} (belonging to the $\{\text{Mo}_{12}\}$ building block): dark blue; Mo^{VI} centres of the two $\{\text{Mo}_2\}$ groups: pink; O: red; H: bright grey; Mo–Mo bonds indicated by dotted lines). Right: Polyhedral representation of **1a**. The four oxygen positions to which a $\{\text{Mo}_2\}$ group attaches are encircled in green.

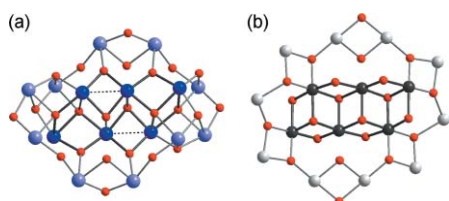


Fig. 2 Schematic comparison of the mixed-valence $\{\text{Mo}_{16}\}$ (a) and $\{\text{Mn}_{16}\}$ (b) frameworks, for clarity only the metal and the bridging oxo positions are shown. Both structures comprise a central fragment of four face-sharing, incomplete M_3O_4 cubanes, highlighted by dark grey bonds and dark blue (Mo) or dark grey (Mn) metal centres. In the case of the $\{\text{Mo}_{16}\}$ cluster this central $\{\text{Mo}_6\}$ fragment contains the four formal Mo^{V} centres that are arranged to form two $\{\text{Mo}^{\text{V}}_2\}$ pairs with short $\text{Mo} \cdots \text{Mo}$ contacts of 2.6 Å, indicated by dashed lines; in the case of the $\{\text{Mn}_{16}\}$ cluster these central metal positions represent the $\{\text{Mn}^{\text{IV}}_6\}$ core.²⁵ These central $\{\text{M}_6\}$ fragments are surrounded by a $\{\text{Mo}^{\text{VI}}_{10}\}$ and $\{\text{Mn}^{\text{III}}_{10}\}$ ring, respectively.

Compound **1** is reasonably stable, both in the solid state and in solution, and it forms metal complexes with divalent transition metal cations and the compounds $(\text{C}_6\text{H}_{13}\text{N}_4)_6[\text{Fe}_2(\text{H}_2\text{O})_8\text{H}_2\text{Mo}_{16}\text{O}_{52}] \cdot 8\text{H}_2\text{O}$ **2**, $(\text{C}_6\text{H}_{13}\text{N}_4)_6[\text{Mn}_2(\text{H}_2\text{O})_8\text{H}_2\text{Mo}_{16}\text{O}_{52}] \cdot 8\text{H}_2\text{O}$ **3** and $(\text{C}_6\text{H}_{13}\text{N}_4)_6[\text{Co}_2(\text{H}_2\text{O})_8\text{H}_2\text{Mo}_{16}\text{O}_{52}] \cdot 8\text{H}_2\text{O}$ **4** can be isolated in good yield. The cluster anions in **2–4** are of approximate C_i symmetry and are based on a $\{\text{Mo}_{16}\}$ fragment where two $[\text{M}(\text{H}_2\text{O})_4]^{2+}$ ($\text{M} = \text{Fe}, \text{Mn}, \text{Co}$) groups are coordinated to inversion symmetry-related sites. Each M^{II} centre binds to two terminal oxo positions of the $\{\text{Mo}_{12}\}$ building block, one of a $\text{Mo}^{\text{V}}\text{O}_6$ and one of an adjoining $\text{Mo}^{\text{VI}}\text{O}_6$ octahedron ($\text{M} \cdots \text{O}(\text{Mo}^{\text{V}})$: 2.129(4) Å; $\text{M} \cdots \text{O}(\text{Mo}^{\text{VI}})$: 2.116(4) Å), see Fig. 3.

Besides compounds **2, 3** and **4**, which can be produced as crystals suitable for single crystal X-ray analysis, crystalline powders were precipitated for the nickel(II) and zinc(II) analogues. X-Ray powder diffraction data indicate that these products represent isomorphous derivatives of compounds **2–4**.

The inherent reactivity of the highly charged cluster anions **1a** causes gradual decomposition and rearrangement reactions when crystals of compound **1** are kept in the reaction solution for some days, after which they re-dissolve and a different solid, $(\text{C}_6\text{H}_{14}\text{N}_4)_{1.5}(\text{C}_7\text{H}_{17}\text{N}_5)_{0.5}[\text{Na}_2\text{Mo}_7\text{O}_{24}(\text{H}_2\text{O})_5]_{\infty} \cdot 4\text{H}_2\text{O}$ **5**, is formed. **5** comprises a zigzag-shaped, one-dimensional anionic coordination polymer of heptamolybdate $[\text{Mo}^{\text{VI}}_7\text{O}_{24}]^{6-}$ units linked by $[(\text{H}_2\text{O})\text{Na}(\mu\text{-OH})_2\text{Na}(\text{H}_2\text{O})_2]^{2+}$ groups, see Fig. 4.

The two sodium positions in the dimer motif $[\text{Na}_2(\text{H}_2\text{O})_5]^{2+}$ are linked *via* two bridging water molecules with a $\text{Na} \cdots \text{Na}$ dis-

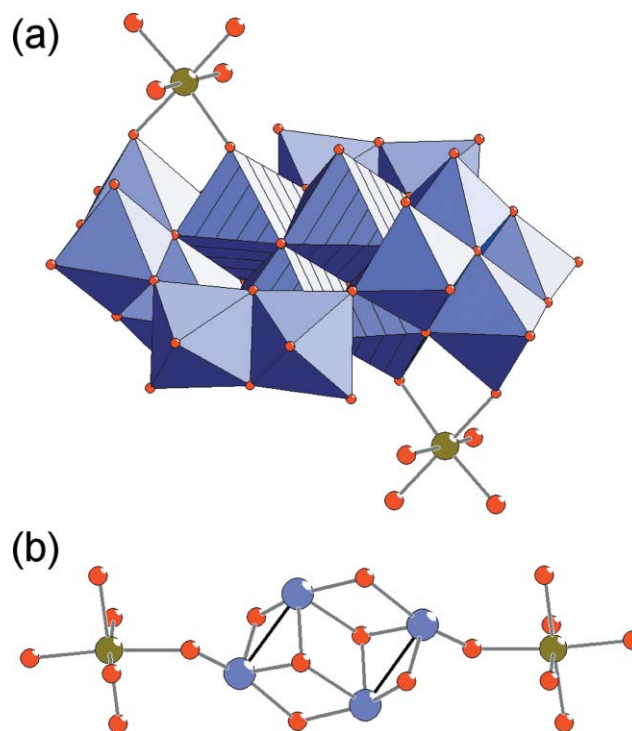


Fig. 3 (a) Representation of the isostructural $\{\text{M}_2\text{Mo}_{16}\}$ -type clusters in **2, 3**, and **4**. The $[\text{H}_2\text{Mo}_4\text{Mo}^{\text{VI}}_{12}\text{O}_{52}]^{10-}$ fragment is shown in polyhedral representation with the four $\text{Mo}^{\text{V}}\text{O}_6$ coordination polyhedra hatched, and the $[\text{M}^{\text{II}}(\text{H}_2\text{O})_4]^{2+}$ groups in ball-and-stick mode. (b) Potential magnetic exchange pathways in $\{\text{M}_2\text{Mo}_{16}\}$ involving the two $\{\text{Mo}^{\text{V}}_2\}$ dimers. Mo–Mo bonds within these dimers are represented by black lines.

tance of ~ 3.5 Å. The dimer binds to the two $\{\text{Mo}_7\}$ fragments in two coordination modes, with one sodium position coordinated to two and the other to three terminal oxo groups of the $\{\text{Mo}_7\}$ fragments with $\text{Na} \cdots \text{O}(\text{Mo})$ distances of 2.450(4) to 2.466(6) Å. One and two terminal water ligands, respectively, complete the slightly distorted octahedral coordination environments of the two sodium cations. In the solid-state structure of **5**, the polymeric $\{\text{Na}_2\text{Mo}_7\}$ strands are sandwiched between layers of HMTA-based cations, see Fig. 5. Interestingly, the cations present in **5** are twofold protonated HTMA and/or an alkylated derivative of HMTA, $N\text{-(H}_2\text{NCH}_2\text{)-HMTA}$, which again is protonated (such an alkylation reaction has been reported by Ojha *et al.*³⁰ and presumably originates from the acid

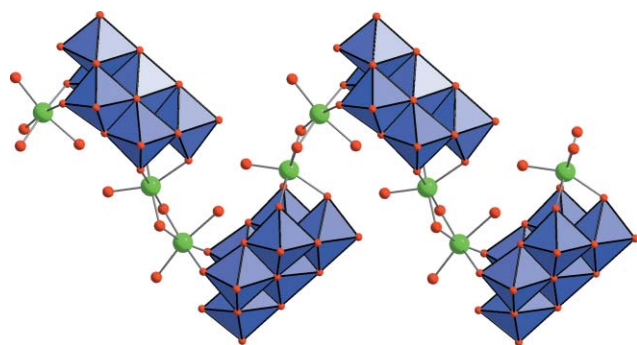
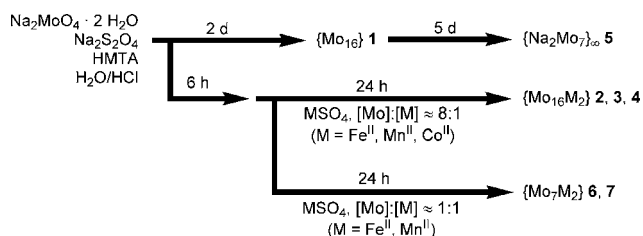


Fig. 4 A section of a polymeric $\{\text{Na}_2\text{Mo}_7\}_\infty$ -type chain in **5** with the heptamolybdate units shown in polyhedral representation (Na: green; O: red). Note the two different coordination modes of the $[\text{Na}_2(\mu\text{-H}_2\text{O})_2(\text{H}_2\text{O})_3]^{2+}$ groups to the heptamolybdate fragments.

catalysed decomposition of some HTMA cations and subsequent alkylation of intact HMTA cations present in solution). For **5**, a ratio of 3 : 1 has been established from elemental and X-ray structure analysis results between the HMTAH_2^{2+} and $N\text{-}(\text{H}_2\text{NCH}_2)\text{-HMTAH}^{2+}$ species. Interestingly, a similar $\{\text{Na}_2\text{Mo}_7\}_\infty$ compound has been described by Yang *et al.*³¹ using a different synthetic strategy that employs MoCl_3 and sodium molybdate as starting materials.

The $\{\text{Mo}_{16}\}$ cluster anion **1a** also decomposes in the presence of divalent transition metal cations in high concentrations, around 5–10 times higher than the concentrations used to produce the $\{\text{M}_2\text{Mo}_{16}\}$ -based compounds **2–4** (see Scheme 1). Under such conditions the isostructural $\{\text{Mo}_7\text{M}_2\}$ -type compounds $(\text{C}_6\text{H}_{13}\text{N}_4)_2[\text{Fe}_2(\text{H}_2\text{O})_9\text{Mo}_7\text{O}_{24}]\cdot 2\text{H}_2\text{O}$ **6** and $(\text{C}_6\text{H}_{13}\text{N}_4)_2[\text{Mn}_2(\text{H}_2\text{O})_9\text{Mo}_7\text{O}_{24}]\cdot 2\text{H}_2\text{O}$ **7** are formed which again are based on individual heptamolybdate fragments that now coordinate to two M^{2+} cations. In the molecular cluster anions **6a**



Scheme 1 Reaction pathways leading to products **1–7**.

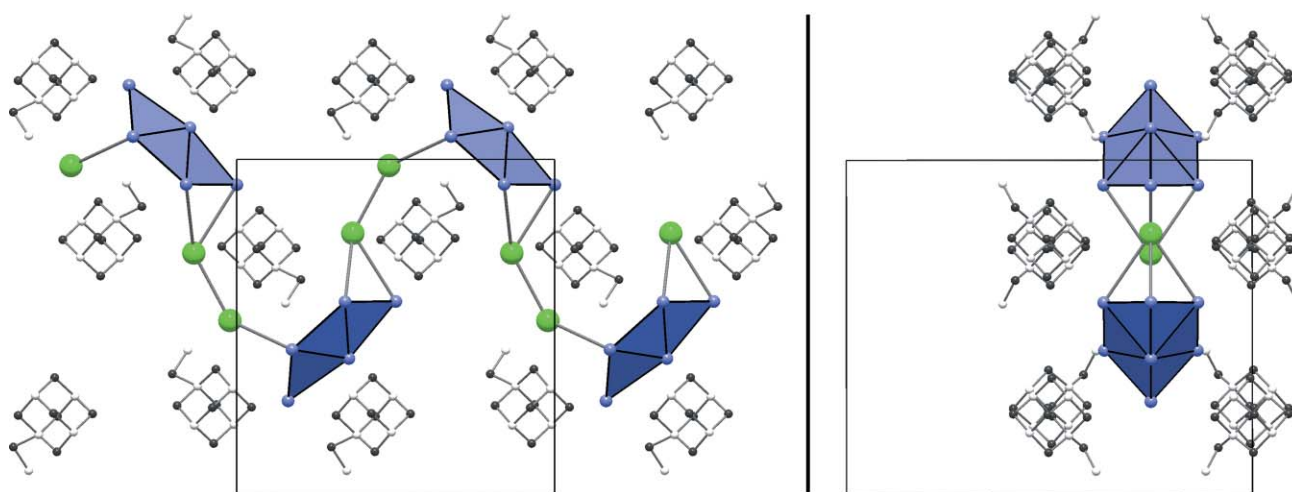


Fig. 5 Simplified representations of the packing of the diprotonated hexamethylenetetramine (HMTAH_2^{2+}) and $N\text{-}(\text{aminomethylene})\text{-hexamethylenetetramine}$ (AMHMTAH_2^{2+}) cations around the zigzag-shaped strands of one polymeric $\{\text{Na}_2\text{Mo}_7\}$ anion, which is shown only by its molybdenum (blue)–sodium (green) skeleton. The aminomethylene groups of the AMHMTAH_2^{2+} cations are found to be underoccupied (occupancy factor: 0.25). C: black; N: bright grey. The left hand view shows a view projected onto the ac plane and the right hand view is projected onto the bc plane.

and **7a**, one of the two Fe^{II} or Mn^{II} centres binds to a terminal oxo position of the $[\text{Mo}_7\text{O}_{24}]^{6-}$ fragment, the other one coordinates to one terminal and one bridging oxo position of a neighbouring MoO_6 octahedron. Correspondingly, five and four terminal water ligands complete the octahedral coordination environments of both M^{2+} centres, see Fig. 6. In addition, compounds **6** and **7** show hydrogen bonding between coordinated water molecules and other terminal oxygen atoms on the molybdate fragment and the protonated HMTA cations, *cf.* Fig. 7.

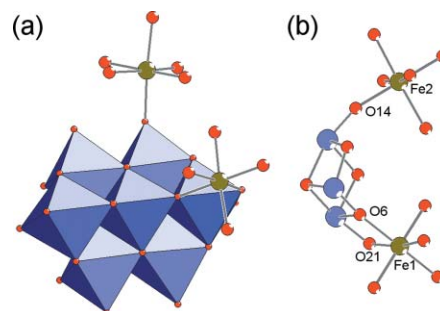


Fig. 6 (a) Structure of the $\{\text{M}_2\text{Mo}_7\}$ anions in **6** and **7** showing the $[\text{Mo}_7\text{O}_{24}]^{6-}$ fragment in polyhedral and the $[\text{M}^{\text{II}}(\text{H}_2\text{O})_4]^{2+}$ and $[\text{M}^{\text{II}}(\text{H}_2\text{O})_5]^+$ groups in ball-and-stick presentation. Note that while one M^{II} centre is coordinating to only one terminal oxo position of the $\{\text{Mo}_7\}$ fragment, the latter is chelating to the second M^{II} centre *via* one terminal and one bridging oxo position of the $\{\text{Mo}_7\}$ fragment. (b) A section of the cluster structure of the $\{\text{Fe}_2\text{Mo}_7\}$ anion **6a** is shown that represents the potential magnetic superexchange pathways. The distances between the Fe^{II} centres and the bridging oxo centres are Fe1–O6 : 2.133(5) Å, Fe1–O21 : 2.155(5) Å, and Fe2–O14 : 2.084(5) Å. The closest inter-molecular Fe–Fe contacts in **6** are $\text{Fe2–Fe2}'$: ~5.54 Å and $\text{Fe1–Fe1}'$: ~5.74 Å.

Magnetic properties

The magnetism of compounds **1–7** was characterized by susceptibility measurements. Weak yet significant antiferromagnetic coupling is observed for all compounds containing spin centres despite the large intramolecular $\text{M} \cdots \text{M}$ distances of *ca.* 11.81 Å in $\{\text{M}_2\text{Mo}_{16}\}$ -based and *ca.* 6.90 Å in $\{\text{M}_2\text{Mo}_7\}$ -based compounds; this illustrates the efficiency of polyoxomolybdates in mediating magnetic superexchange. In the $\{\text{M}_2\text{Mo}_{16}\}$ -type compounds **2–4** the shortest superexchange pathways are of the type $\text{M}^{\text{II}}\text{–O–Mo}^{\text{V}}\text{–Mo}^{\text{V}}\text{–O–Mo}^{\text{V}}\text{–O–M}^{\text{II}}$ (assuming a metal–metal bond between the Mo centres of a $\{\text{Mo}_2\text{V}_2\}$ dimer), Fig. 3b, while $\text{M}^{\text{II}}\text{–O–Mo}^{\text{VI}}\text{–O–Mo}^{\text{VI}}\text{–O–M}^{\text{II}}$ pathways, Fig. 5b,

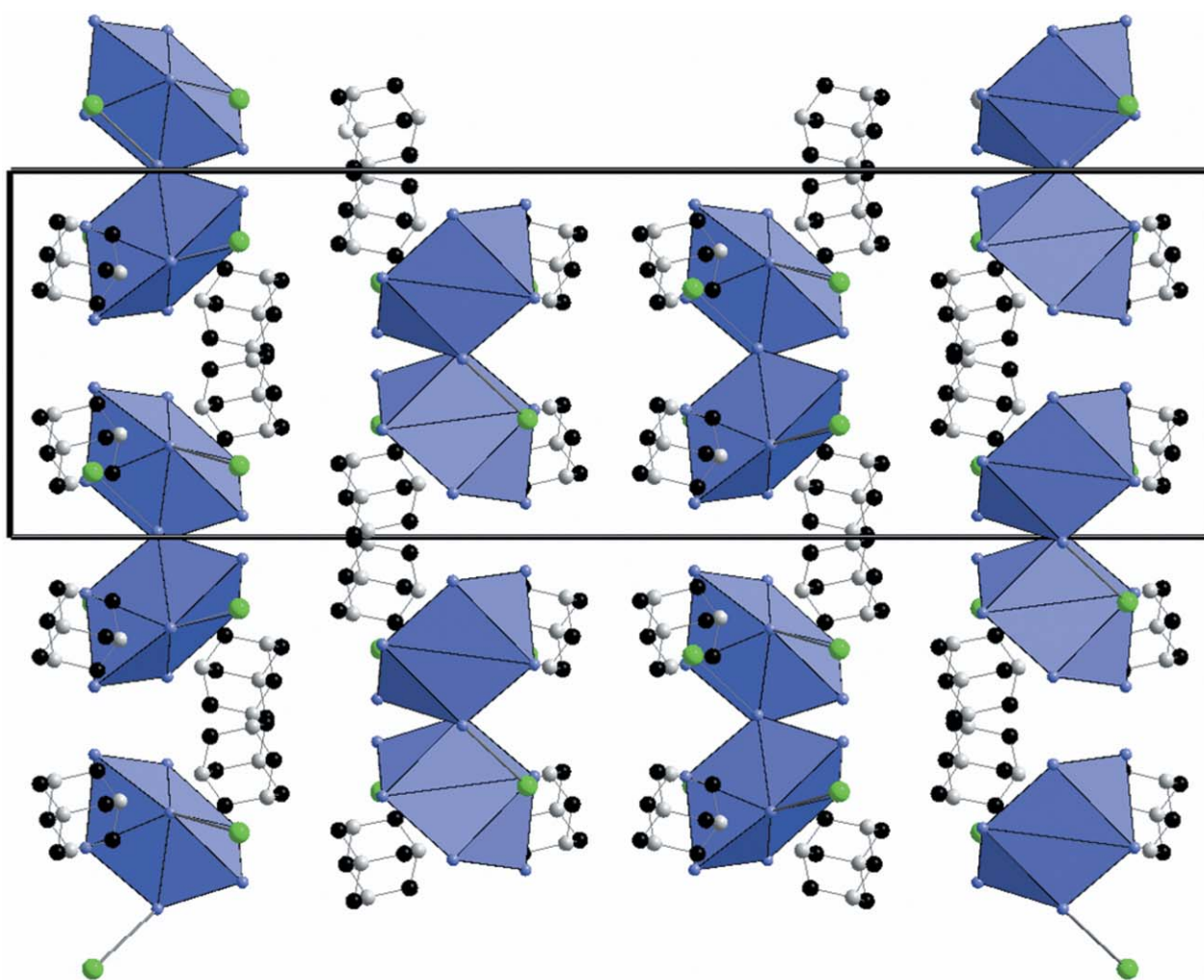


Fig. 7 Packing of the $\{M_2Mo_7\}$ anions and the HMTAH⁺ cations in the crystal structure of **6** and **7**, seen along the *c* axis. The dimensions of one unit cell are emphasized. The heptamolybdate fragments are represented by blue polyhedra with the appended Fe^{II}/Mn^{II} centres in green. C: black; N: bright grey.

are present in the $\{M_2Mo_7\}$ -type compounds **6** and **7**. For the observed temperature range (2–290 K) intermolecular dipole–dipole coupling is negligible due to the wide separation of M centres in neighbouring cluster anions. Susceptibility data were corrected for diamagnetic contributions established from compounds **1** and **5** for the $\{M_2Mo_{16}\}$ and $\{M_2Mo_7\}$ compounds, respectively. For all dimeric compounds an isotropic Heisenberg Hamiltonian $H = -JS_1S_2$ has been used to model the experimental data, for compounds containing Fe(II) and Co(II) centres; anisotropy terms ($S_1DS_1 + S_2DS_2$ where *D* represents the single-ion anisotropy) were also included. All compounds show weak intramolecular antiferromagnetic coupling, as can be seen from all data curves showing the temperature dependence of $\chi_{mol}T$ at 0.5 Tesla, see Fig. 8. For the Mn^{II} ($S = 5/2$) compounds **3** and **7**, very weak coupling is observed with $J/k = -0.06$ K for **3** and $J/k = -0.15$ K for **7**, with a g_{iso} factor of 1.99 for **3** and 2.01 for **7**. In the case of the Fe^{II} ($S = 2$)-based compounds **2** and **6** an anisotropy value of $D/k = 8.0$ K was adopted to accommodate effects from the zero-field splitting of the 3T_2 term of the high-spin $3d^6$ Fe^{II} centres in an octahedral field. This yielded best fits to the experimental data with $J/k = -0.8$ K and $g_{iso} = 2.03$ for **2** and $J/k = -2.1$ K and $g_{iso} = 2.15$ for **6**. For the Co^{II} ($S = 3/2$) compound no satisfying fit could be obtained, which most likely is due to the strong anisotropy associated with Co^{II} centres in octahedral coordination environments.

Electronic properties

In order to explore the reactivity of the highly charged cluster anion **1a** density functional theory calculations were performed

on both **1a** and its Zn(II) derivative $[Zn_2(H_2O)_8H_2Mo_{16}O_{52}]^{6-}$. Overall, the surface charge distribution as defined by the atomic net charges of the terminal oxo positions shows pronounced charge maxima and minima. Class-2 (Löwdin) atomic charges of these 26 positions differ by up to 22% from the average of -0.532 , and by up to 26% from the average of -0.494 for the 14 μ_2 -oxo positions, compared to the maximum differences of 8% from the average of -0.493 for the 12 $\mu_{3/4}$ -oxo positions, see Fig. 7. It is interesting that the reaction of **1a** with divalent metal cations binds them to one terminal oxo position of a formal Mo^V centre and one terminal oxo position of an adjacent Mo^{VI} centre (O–O = 2.99 Å), although these positions, out of all terminal oxo pairs with O–O distances < 3.3 Å that allow a chelating coordination mode to the M^{II} centres, show relatively low negative net charges of -0.41 (Mo^VO), the least negatively charged oxo positions) and -0.57 (Mo^{VI}O). The four Mo(4d) electrons in **1a** and **2a–7a** are mostly localized over the two central $\{Mo_2\}$ dimers, and correspondingly the orbital overlap between these positions is significant, indicating a single metal–metal bond. Moreover, the net atomic charges of the oxygen centres in **2a–7a**, especially of the terminal oxo positions, are distributed in a more uniform way compared to **1a**. This greater uniformity of net charges is reflected by the maximum deviations from the average values: 16% from the average value of -0.487 for the 22 terminal oxo positions, 20% from the average of -0.469 for the 12 μ_2 -oxo positions (excluding the oxo positions to which the Zn centres are bound), and 12% from the average of -0.506 for all of the 14 $\mu_{3/4}$ -oxo positions, see also Fig. 9. Thus, possible reasons for the apparent absence of species of the

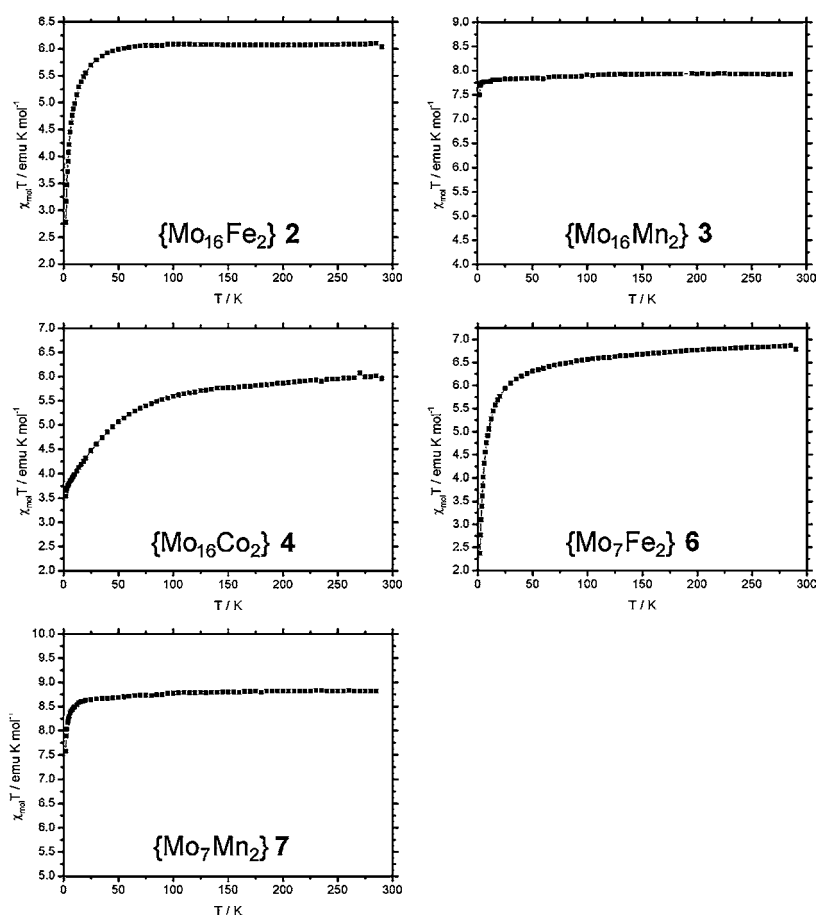


Fig. 8 Magnetic susceptibility data (temperature dependence of $\chi_{\text{mol}}T$ at 0.5 Tesla) for compounds **2**, **3**, **4**, **6**, and **7**.

type $\{M^{\text{II}}_n\text{Mo}_{16}\}$ with $n > 2$ are either the reduced total charge of the anion or the lack of additional reactive ‘‘hot spots’’, *i.e.*, surface charge maxima.

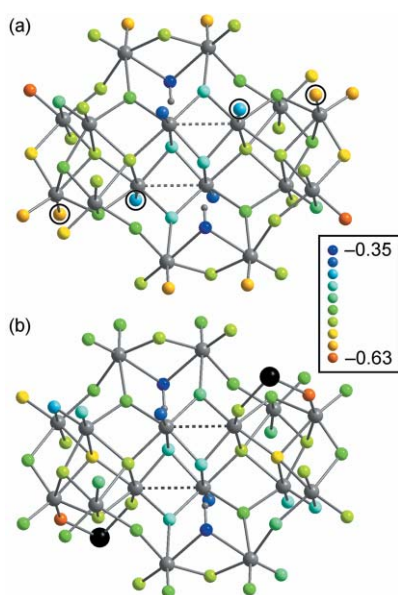


Fig. 9 Colour-coded distribution of calculated atomic net charges of the oxygen positions in **1a** (a) and $\{\text{Zn}_2\text{Mo}_{16}\}$ (b) with the range of Löwdin partial charges assigned in the legend, illustrating the change in oxo position charges when the $\{\text{Mo}_{16}\}$ anion coordinates to two M^{II} centres. The two pairs of vicinal terminal oxygen positions in **1a** to which divalent transition metal cations are coordinated in the $\{\text{M}_2\text{Mo}_{16}\}$ cluster anions **2a**, **3a**, and **4a** are encircled in black. In (b), the Zn^{II} positions are shown in black without the water ligands.

Conclusions

We have demonstrated the production and complexation of an unusual mixed-valence polyoxomolybdate, which contains sixteen molybdenum centres and displays a non-spherical structure, but is sufficiently reactive to form complexes with other divalent transition metals. This $\{\text{Mo}_{16}\}$ cluster appears to be assisted in its formation by the use of bulky organo cations and we have shown that it can react with a number of electrophiles to form the corresponding $\{\text{Mo}_{16}\text{M}_2\}$ adducts. Investigation of the structures using DFT demonstrates the existence of nucleophilic ‘hot-spots’ but do not predict the sites for electrophile coordination, and the magnetic investigation of the paramagnetic $\{\text{Mo}_{16}\text{M}_2\}$ adducts illustrates the efficiency of polyoxomolybdates in mediating magnetic superexchange. Furthermore we discovered that the $\{\text{Mo}_{16}\}$ and $\{\text{Mo}_{16}\text{M}_2\}$ adducts are unstable in solution for long periods and decompose to smaller $\{\text{Mo}_7\}$ and $\{\text{Mo}_7\text{M}_2\}$ units. The potential to utilise the unstable $\{\text{Mo}_{16}\}$ and $\{\text{Mo}_{16}\text{M}_2\}$ as precursors to other cluster types and building blocks is now under investigation.

Acknowledgements

This work was supported by the Leverhulme Trust (London), the EPSRC, the Royal Society, and the University of Glasgow. The EPSRC provided funds for the X-ray diffractometer.

References

- 1 L. Cronin, High Nuclearity Polyoxometalate Clusters, in *Comprehensive Coordination Chemistry 2*, Elsevier–Pergamon, New York, 2004, 7th edn., p. 1.
- 2 L. Cronin, C. Beugholt, E. Krickemeyer, M. Schmidtman, H. Bögge, P. Kögerler, T. K. K. Luong and A. Müller, *Angew. Chem., Int. Ed.*, 2002, **41**, 2805.
- 3 I. V. Kozhevnikov, *Chem. Rev.*, 1998, **98**, 171.

- 4 J. T. Rhule, W. A. Neiwert, K. I. Hardcastle, B. T. Do and C. L. Hill, *J. Am. Chem. Soc.*, 2001, **123**, 12101.
- 5 A. Müller, M. Luban, C. Schröder, R. Modler, P. Kögerler, M. Axenovich, J. Schnack, P. Canfield, S. Bud'ko and N. Harrison, *ChemPhysChem*, 2001, **2**, 517.
- 6 A. Müller, P. Kögerler and A. W. M. Dress, *Coord. Chem. Rev.*, 2001, **222**, 193.
- 7 K. F. Aguey-Zinsou, P. V. Bernhardt, U. Kappler and A. G. McEwan, *J. Am. Chem. Soc.*, 2003, **125**, 530.
- 8 D. A. Judd, J. H. Nettles, N. Nevins, J. P. Snyder, D. C. Liotta, J. Tang, J. Ermolieff, R. F. Schinazi and C. L. Hill, *J. Am. Chem. Soc.*, 2001, **123**, 886.
- 9 H. D. Zeng, G. R. Newkome and C. L. Hill, *Angew. Chem., Int. Ed.*, 2000, **39**, 1772.
- 10 M. T. Pope and A. Müller, *Angew. Chem., Int. Ed. Engl.*, 1991, **30**, 34.
- 11 F. Ogliaro, S. P. de Visser, S. Cohen, P. K. Sharma and S. Shaik, *J. Am. Chem. Soc.*, 2002, **124**, 2806.
- 12 T. Yamase, *Chem. Rev.*, 1998, **98**, 307.
- 13 A. Müller, P. Kögerler and C. Kuhlmann, *Chem. Commun.*, 1999, 1347.
- 14 K. Wassermann, M. H. Dickman and M. T. Pope, *Angew. Chem., Int. Ed. Engl.*, 1997, **36**, 1445.
- 15 D. Hagrman, P. J. Hagrman and J. Zubieta, *Angew. Chem., Int. Ed.*, 1999, **38**, 3165; S. S. Kuduva, N. Avarvari and M. Fourmigue, *J. Chem. Soc., Dalton Trans.*, 2002, 3686.
- 16 P. Mialane, A. Dolbecq, L. Lisnard, A. Mallard, J. Marrot and F. Secheresse, *Angew. Chem., Int. Ed.*, 2002, **41**, 2398.
- 17 T. Hori, O. Tamada and S. Himeno, *J. Chem. Soc., Dalton Trans.*, 1989, 1491; S. Juraja, T. Vu, P. J. S. Richardt, A. M. Bond, T. J. Cardwell, J. D. Cashion, G. D. Fallon, G. Lazarev, B. Moubaraki, K. S. Murray and A. G. Wedd, *Inorg. Chem.*, 2002, **41**, 1072.
- 18 M. I. Khan, A. Müller, S. Dillinger, H. Bögge, Q. Chen and J. Zubieta, *Angew. Chem., Int. Ed. Engl.*, 1993, **32**, 1780.
- 19 M. I. Khan, Q. Chen, J. Salta, C. J. O'Connor and J. Zubieta, *Inorg. Chem.*, 1996, **35**, 1880.
- 20 D.-L. Long, P. Kögerler, L. J. Farrugia and L. Cronin, *Angew. Chem., Int. Ed.*, 2003, **42**, 4180.
- 21 D.-L. Long, P. Kögerler and L. Cronin, *Angew. Chem., Int. Ed.*, 2004, **43**, 1817.
- 22 D.-L. Long, H. Abbas, P. Kögerler and L. Cronin, *J. Am. Chem. Soc.*, 2004, **126**, 13880.
- 23 G. M. Sheldrick, *SHELXL-97. Program for Crystal structure analysis*, University of Göttingen, Germany, 1997.
- 24 L. J. Farrugia, *J. Appl. Crystallogr.*, 1999, **32**, 837.
- 25 D. J. Price, S. R. Batten, B. Moubaraki and K. S. Murray, *Chem. Commun.*, 2002, 762.
- 26 W. B. Yang, C. Z. Lu, X. Lin and H. H. Zhuang, *Inorg. Chem.*, 2002, **41**, 452.
- 27 C. du Peloux, P. Mialane, A. Dolbecq, J. Marrot and F. Secheresse, *Angew. Chem., Int. Ed.*, 2002, **41**, 2808.
- 28 A. Müller, C. Kuhlmann, H. Bögge, M. Schmidtman, M. Baumann and E. Krickemeyer, *Eur. J. Inorg. Chem.*, 2001, 2271.
- 29 R. Neier, C. Trojanowski and R. Mattes, *J. Chem. Soc., Dalton Trans.*, 1995, 2521.
- 30 T. Duraisamy, N. Ojha, A. Ramanan and J. J. Vittal, *Chem. Mater.*, 1999, **11**, 2339.
- 31 W. B. Yang, C. Z. Lu and H. H. Zhuang, *Chin. J. Struct. Chem.*, 2002, **21**, 168.
- 32 A. Müller and C. Serain, *Acc. Chem. Res.*, 2000, **33**, 2.
- 33 I. D. Brown, in *Structure and Bonding in Crystals*, eds. M. O'Keeffe and A. Navrotsky, Academic Press, New York, 1981, vol. II, pp. 1–30.